β-tin→Imma→sh Phase Transitions of Germanium

Xiao-Jia Chen, Chao Zhang, Yue Meng, Rui-Qin Zhang, Hai-Qing Lin, Viktor V. Struzhkin, and Ho-kwang Mao

β-tin→$Imma$→sh Phase Transitions of Germanium

Xiao-Jia Chen,[1] Chao Zhang,[2] Meng Yue,[3] Rui-Qin Zhang,[2] Hai-Qing Lin,[4] Viktor V. Struzhkin,[1] and Ho-kwang Mao[1]

[1] *Geophysical Laboratory, Carnegie Institution of Washington, Washington, DC 20015, USA*
[2] *Department of Physics and Materials Science, City University of Hong Kong, Hong Kong, China*
[3] *High-Pressure Collaborative Access Team, Carnegie Institution of Washington, Argonne, Illinois 60439, USA*
[4] *Department of Physics, Chinese University of Hong Kong, Hong Kong, China*

New paths were designed for the investigations of the β-tin→$Imma$→sh phase transitions in nanocrystalline Ge under conditions of hydrostatic stress. A second-order transition between the β-tin and $Imma$ phases was identified at 66 GPa, and a first-order transition between the $Imma$ and sh phases was determined at 90 GPa. Superconductivity was obtained up to 190 GPa using the acquired structural data in first principles calculations. This provides evidence that the standard electron-phonon coupling mechanism is responsible for superconductivity in Ge, as evidenced by the good agreement between the calculations and existing experiments.

Due to their fundamental nature and technological importance, the high-pressure behavior of group-IVa elements has been one of the most active areas of high-pressure research. The recent discovery of superconductivity at ambient pressure in heavily doped elements [1–3] has renewed significant interest in these materials due to their possible application in superconducting data processing for next-generation computer architectures [4]. Germanium (Ge) has many advantages over silicon (Si) [5]: higher intrinsic electron mobilities, allowing for faster circuits; more prominent quantum-confinement effects for photoluminescence studies and bandgap control of the nanostructures; and compatibility with high-dielectric-constant materials, enabling integration with current semiconductor processing technology. The structural properties of Ge at ambient conditions and at high pressure show some similarity with those of Si [6], but the transition pressures of Ge are higher, which is attributed to its core d electrons [7, 8]. Upon compression, the Ge semiconducting diamond structure transforms to a metallic β-tin phase with space group $I4_1/amd$ near 10 GPa [9] and then, via the $Imma$ phase [10], into the simple hexagonal (sh) structure with space group $P6/mmm$ [11]. Further compression yields the orthorhombic $Cmca$ phase near 100 GPa and a hcp structure above 170 GPa [12]. This picture of a series of phase transitions to high-symmetry structures of increasing coordination signifies Ge as an ideal material for experimental and theoretical studies.

The β-tin→$Imma$ and $Imma$→sh phase transitions are two of the most studied solid-solid phase transitions in condensed matter physics, both from an experimental and a theoretical point of view [6, 7, 10, 13–16]. Both of these phase transitions in Ge have been suggested as being either second order [7] or first order [13]. An elastic instability analysis indicates that the β-tin→$Imma$ transition is second-order [14], while recent work [15] reveals that the order for the β-tin→$Imma$ transition cannot be definitely determined from theory, although a first-order $Imma$→sh phase transition can be identified computationally. Only one data point is available for the $Imma$ phase [10], making determination of the transitions to and from this phase as well as determination of their orders unrealistic. Meanwhile, the transition pressures have been found to be very sensitive to the degree of nonhydrostaticity [9] as well as to particle sizes [17]. Accurate structural information on the β-tin→$Imma$→sh phase-transition sequence with nanocrystalline samples under conditions of hydrostatic pressure is highly desirable, not only for understanding the phase transitions themselves but also for studying the associated superconductivity, which has not yet been studied beyond the β-tin phase [18–20]. This structural behavior is also of considerable interest for clarifying the unanswered questions surrounding the superconducting coupling mechanism, as well as the relationship between the structures and properties of the heavily doped group-IVa elements [21], which has been obscured due to complicating factors of disorder and dopant homogeneity.

In this Letter, we address the aforementioned issues with fine structural investigations on compressed Ge nanocrystalline samples in a hydrostatic environment. A second-order transition between the β-tin and $Imma$ phases was identified at 66 GPa and first-order transition between the $Imma$ and sh phases was observed at 90 GPa. These two transition pressures are in good agreement with the theoretical predictions made by Ribeiro and Cohen [13]. Superconductivity of metallic Ge is obtained within first principles calculations using the obtained structures. A good agreement between the calculations and experiments for the β-tin phase indicates that the elemental semiconductor Ge is indeed a standard electron-phonon coupling superconductor.

Structural information was obtained through the angle-dispersive powder X-ray diffraction experiments performed with an X-ray beam with wavelength of 0.36121 Å at beamline 16ID-B, the Advanced Photon Source of the Argonne National Laboratory. Pressure was generated in a sample chamber of tungsten gasket with initial dimensions of 50

μm in diameter and 30 μm thick by using a pair of beveled diamond anvils having a 100 μm diameter flat and a 10° bevel out from the 300 μm total culet diameter. 99.99% purity germane (GeH$_4$) was loaded into the diamond anvil cell at low temperatures. After gradually applying pressure up to 17 GPa, we found that GeH$_4$ decomposes into Ge and H$_2$ mixture, which was confirmed from both Raman scattering and X-ray diffraction measurements. The linear dimensions of particles at 17 GPa were estimated from the Scherrer equation to be less than 10 nm. The appearance of H$_2$ provides a hydrostatic environment for nanocrystalline Ge. These conditions ensure the accurate determination of the transition pressures [9, 17]. The diffraction patterns of the sample were collected from the center of the gasket hole and those from the nearby platinum were used to gauge pressure by using the equation of state [22]. The data were integrated azimuthally using FIT2D [23] and analyzed by the Rietveld method using the FULLPROF program [24]. Figure 1 shows the X-ray patterns and refined results of Ge at selected pressures. The patterns measured for 41, 84, and 105 GPa can be well refined to the $I4_1/amd$, $Imma$, and $P6/mmm$ space group, respectively. These results are consistent with prior reports on the structures in this pressure range [9–11].

Figure 2 shows the atomic arrangements of the three interesting metallic phases of note, as well as the lattice parameters of Ge as a function of pressure. These data are used to identify the β-tin $\rightarrow Imma \rightarrow$ sh phase transitions in Ge. The structural transformations are clearly seen from the evolution of both the lattice parameters and their ratios c/a. In the β-tin phase above 10 GPa, Ge has $I4_1/amd$ symmetry with Ge occupying Wyckoff $4a$ positions, shown in Fig. 2(a). The Ge 3D network can be taken as constituted by two crossed Ge zigzag chains, located in (100) and (010) planes, respectively. As the pressure is increased, the relative positions of Ge atoms in the zigzag chains do not change, while the lattice parameters decrease significantly. Interestingly, the c/a ratio keeps a constant value (0.547) [Fig. 2(e)], consistent with other experimental and theoretical work [11, 13].

Upon entering $Imma$, the neighboring Ge atoms in both zigzag chains move in opposite directions projected in the c axis [Fig. 2(b)]. As a result, the two Ge zigzag chains show different behaviors. The Ge-Ge bond angle of zigzag chain in the (010) plane increases to nearly 180°, while the Ge-Ge bond angle of the other chain in the (100) plane tends to 90°. As seen from Fig. 2(d), the movement of Ge atoms also leads to expansion of the a axis but contraction of the b axis up to 90 GPa. The c/a ratio of this phase reduces to 0.540 [Fig. 2(e)], accordingly.

When the Ge zigzag chain in the (010) plane becomes straight and the other chain becomes a right angle, Ge transforms to an sh phase. The lines in Fig. 2(c) draw the primitive cell of the sh phase, which contains only one Ge atom. The lattice parameters for this phase can be expressed in orthorhombic setting as $a_O = 2c_H$, $b_O = \sqrt{3}a_H$, and $c_O = a_H$. Compared with the β-tin and $Imma$ phases, the lattice parameters of the sh phase in the orthorhombic setting slowly decrease with pressure while the c/a ratio appears stable [Figs. 2(d)-(e)].

The area conserving quantity $\sqrt{ab}$ follows smoothly from the a axis of the β-tin phase across the transition but has a kink between the $Imma$ and sh phases. There is no apparent change in compressibility of the c axis among these phases. These features contribute to the continue change of the molar volume with pressure in the β-tin $\rightarrow Imma$ transition and different compressibilities in the $Imma$ and the sh as shown in Fig. 3. There, the $P - V$ data for the lower (higher) pressure phases are taken from Ref. [9] ([12]) and only one data point for $Imma$ from Ref. [10] is available for comparison. The apparent volume changes across the $diamond \rightarrow \beta$-tin, sh $\rightarrow Cmca$, and $Cmca \rightarrow$ hcp transitions indicate their first-order nature. Our data points in the $Imma$ phase follow a nice evolution path which is coincident with the point from Ref. [10].

We have examined theoretically the structural stability of metallic Ge from first-principles pseudopotential plane-wave method based on the density functional perturbation theory [25] implemented in the Quantum-Espresso package [26]. We used Perdew-Burke-Ernzerhof [27] functional within generalized gradient approximation in the Troullier-Martins norm-conserving scheme [28]. The electronic wave function and the charge density were expanded with kinetic energy cutoffs of 50 and 300 Ry, respectively. The results are shown in Fig. 3. The agreement between the experimental $P - V$ data and the calculated results are excellent for the β-tin, $Imma$, and sh phase. There is also a fair agreement between the theory and measurement for the $Cmca$ and hcp phases.

The order of the phase transition can be determined through the group-subgroup relations [16, 29]. If the order of the point group of one phase is one half (one third) of the order of the point group of the other phase, the phase transition is second-order (first-order). The order of the point group mmm of the $Imma$ phase is 8. Because the order of the point group $4/mmm$ of the β-tin phase is 16 and the order of the point group $6/mmm$ of the sh structure is 24, the β-tin $\rightarrow Imma$ transition has to be second-order while the $Imma \rightarrow$ sh transition is first-order. An independent assessment of the β-tin and $Imma$ transformation is provided by the order parameter − the spontaneous strain $e_{ss} = (a - b)/(a + b)$. According to Landau's theory of second-order phase transitions, the order parameter should be proportional to $(P - P_c)^{1/2}$ with P_c being the transition pressure. Plotting e_{ss}^2 vs pressure, as in Fig. 4, our data appear very linear up to 78 GPa. A linear fit provides a value of P_c of 66 GPa, supporting the second-order transition characteristic. Both this transition pressure and the one between the $Imma$ and sh phases agree well to theoretical calculations [13].

Now we examine superconductivity in metallic Ge using the superconducting transition temperature T_c equation modified by Allen ad Dynes [30], taking a typical value of 0.1 for the Coulomb pseudopotential μ^*. The electron-phonon coupling matrix elements for different phases have been computed in the first Brillouin zone on a reasonable q-point mesh obtained from a sufficiently dense k-point Monkhorst-Pack mesh [31].

Figure 5 shows the pressure dependence of the logarithmic average phonon frequency ω_{log}, electron-phonon coupling λ, and T_c for the metallic Ge phases. In each phase, the calculated T_c and λ decrease with pressure, while ω_{log} increases monotonically with pressure. This suggests that the electronic stiffness of λ dominates the T_c behavior and the soft phonon modes does not noticeably affect T_c. This is somewhat different from the case of Si in which the softening of phonon modes also plays an important role in superconductivity [32]. In the β-tin phase, the calculated T_c considerably decreases with pressure, from 4.7 K at 10.7 GPa (no shown) to $\sim$3 K at $\sim$25 GPa, in good agreement with existing experiments [18–20]. For the $Imma$ phase, the predicted T_c further decreases under pressure, but exhibits a much smaller slope. T_c increases slightly from the $Imma$ to the sh phase and then decreases slowly with increasing pressure. A similar behavior for T_c in the sh phase was also predicted by Martins and Cohen [33] but with a relatively high range of 2-7 K. Unlike the case of Si where T_c exhibits a sharp rise [32], T_c in the $Cmca$ Ge exhibits almost the same behavior as in the sh phase until finally reaching 0.1 K at 190 GPa in the hcp phase. Over the whole pressure range studied, T_c correlates well with λ, indicating the phonon-mediated superconductivity in dense Ge.

In summary, we have obtained structural information on the β-tin$\rightarrow Imma \rightarrow$sh phase transitions in Ge using nanocrystalline samples and at hydrostatic conditions. The transition between the β-tin and $Imma$ phases and the one between the $Imma$ and sh phases are identified to be second order and first order with the transition pressure of 66 GPa for the former and 90 GPa for the latter. The structural data are used to predict superconductivity up to 200 GPa using first principles calculations. Good agreement between the calculations and existing experiments provides evidence for the phonon-mediated mechanism of superconductivity for element Ge.

[1] E. A. Ekimov, V. A. Sidorov, E. D. Bauer, N. N. Mel'nik, N. J. Curro, J. D. Thompson, and S. M. Stishov, Nature (London) **428**, 542 (2004).
[2] E. Bustarret, C. Marcenat, P. Achatz, J. Kačmarčik, F. Lévy, A. Huxley, L. Ortéga, E. Bourgeois, X. Blase, D. Débarre, and J. Boulmer, Nature (London) **444**, 465 (2006).
[3] T. Herrmannsdörfer, V. Heera, O. Ignatchik, M. Uhlarz, A. Mücklich, M. Posselt, H. Reuther, B. Schmidt, K.-H. Heinig, W. Skorupa, M. Voelskow, C. Wündisch, R. Skrotzki, M. Helm, and J. Wosnitza, Phys. Rev. Lett. **102**, 217003 (2009).
[4] K. L. Ekinci and M. L. Roukes, Rev. Sci. Instrum. **76**, 061101 (2005).
[5] C. Claeys and E. Simoen, *Germanium-Based Technologies from Materials to Devices* (Elsevier, Amsterdam, 2007).
[6] A. Mujica, A. Rubio, A. Munoz, and R. J. Needs, Rev. Mod. Phys. **75**, 863 (2003).
[7] S. P. Lewis and M. L. Cohen, Solid State Commun. **89**, 483 (1994).
[8] K. J. Chang and M. L. Cohen, Phys. Rev. B **34**, 8581 (1986).
[9] C. S. Menoni, J. Z. Hu, and I. L. Spain, Phys. Rev. B **34**, 362 (1986).
[10] R. J. Nelmes, H. Liu, S. A. Belmonte, J. S. Loveday, M. I. McMahon, D. R. Allan, D. Häusermann, and M. Hanfland, Phys. Rev. B **53**, R2907 (1996).
[11] Y. K. Vohra, K. E. Brister, S. Desgreniers, A. L. Ruoff, K. J. Chang, and M. L. Cohen, Phys. Rev. Lett. **56**, 1944 (1986).
[12] K. Takemura, U. Schwarz, K. Syassen, M. Hanfland, N. E. Christensen, D. L. Novikov, and I. Loa, Phys. Rev. B **62**, R10603 (2000).
[13] F. J. Ribeiro and M. L. Cohen, Phys. Rev. B **62**, 11388 (2000).
[14] M. Hebbache, M. Mattesini, and J. Szeftel, Phys. Rev. B **63**, 205201 (2001).
[15] K. Gaál-Nagy, P. Pavone, and D. Strauch, Phys. Rev. B **69**, 134112 (2004).
[16] H. Katzke, U. Bismayer, and P. Tolédano, Phys. Rev. B **73**, 134105 (2006).
[17] H. Wang, J. F. Liu, Y. He, Y. Wang, W. Chen, J. Z. Jiang, J. S. Olsen, and L. Gerward, J. Phys.: Condens. Matter **19**, 156217 (2007).
[18] J. Wittig, Z. Phys. **195**, 215 (1966).
[19] H. Kawamura and K. Tachikawa, J. Phys. Soc. Jpn. **57**, 3289 (1988).
[20] H. B. Cui, D. Graf, J. S. Brooks, and H. Kobayashi, Phys. Rev. Lett. **102**, 237001 (2009).
[21] X. Blase, E. Bustarret, C. Chapelier, T. Klein, and C. Marcenat, Nature Mater. **8**, 375 (2009).
[22] N. C. Holmes, J. A. Moriarty, G. R. Gathers, and W. J. Nellis, J. Appl. Phys. **66**, 2962 (1989).
[23] A. P. Hammersley, S. O. Svensson, M. Hanfland, A. N. Fitch, and D. Hausermann, High Press. Res. **14**, 235 (1996).

[24] J. Rodrguez-Carvajal, Physica B **192**, 55 (1993).

[25] S. Baroni, S. de Gironcoli, A. Dal Corso, and P. Giannozzi, Rev. Mod. Phys. **73**, 515 (2001).

[26] P. Giannozzi, et al., J. Phys.: Condens. Matter **21**, 395502 (2009).

[27] J. P. Perdew, K. Burke, and M. Ernzerhof, Phys. Rev. Lett. **77**, 3865 (1996).

[28] N. Troullier and J. L. Martins, Phys. Rev. B **43**, 1993 (1991).

[29] N. Boccara, Ann. Phys. (New York) **47**, 40 (1968).

[30] P. B. Allen and R. C. Dynes, Phys. Rev. B **12**, 905 (1975).

[31] H. J. Monkhorst and J. D. Pack, Phys. Rev. B **13**, 5188 (1976).

[32] D. Erskine, P. Y. Yu, K. J. Chang, and M. L. Cohen, Phys. Rev. Lett. **57**, 2741 (1986).

[33] J. L. Martins and M. L. Cohen, Phys. Rev. B **37**, 3304 (1988).

FIG. 1: (color online) X-ray powder diffraction patterns of solid Ge at pressure of 41, 84, and 105 GPa. The refined lattice parameters for the corresponding space groups are given. The points represent the measured intensities and the lines the results of profile refinements. The positions of the Bragg reflections are marked by vertical lines and the difference profiles are shown at the bottoms.

FIG. 2: (color online) Atomic arrangement of the (a) β-tin, (b) $Imma$, and (c) sh structures of Ge. (d) Pressure dependence of the lattice parameters and (e) the c/a ratios of Ge. In all plots, error bars are smaller than the symbols. The vertical dashed lines denote the phase boundaries.

FIG. 3: (color online) Molar volume vs pressure for Ge. The open diamonds for the diamond phase and the left-pointing triangles for the β-tin phase are from Ref. [9]. The open cycle for the $Imma$ phase is from Ref. [10]. The downward-pointing triangles for the $Cmca$ phase and the squares for the hcp phase are from Ref. [12]. The solid lines are the theoretical predictions for the metallic phases. The vertical dashed lines indicate the phase boundaries determined from the experiments (the former three) and theory (the latter two).

FIG. 4: (color online) Pressure dependence of the square of the spontaneous strain, defined as $(a-b)/(a+b)$, for Ge. The line shows a linear fit of the form $A^2(P-P_c)$ yielding a transition pressure P_c. The open cycle is from Ref. [10].

FIG. 5: (color online) Pressure dependence of (a) the calculated logarithmic average phonon frequency ω_{log}, (b) the electron-phonon coupling parameter λ, and (c) the superconducting transition temperature T_c for metallic Ge. The T_c values indicated by the stars, open triangles, and open cycles are taken from Ref. [18], Ref. [19], and Ref. [20], respectively.
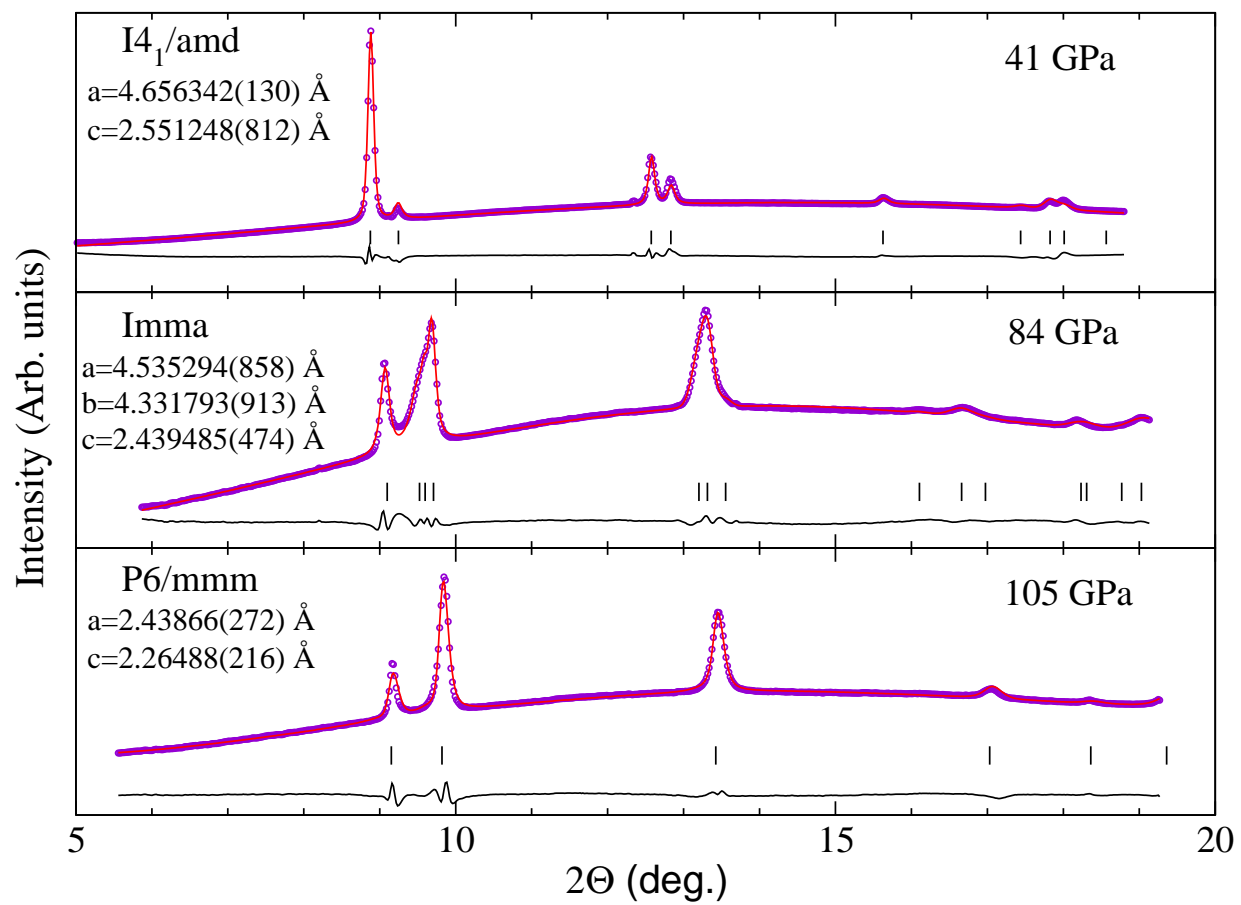
I4$_1$/amd
a=4.656342(130) Å
c=2.551248(812) Å
41 GPa

Imma
a=4.535294(858) Å
b=4.331793(913) Å
c=2.439485(474) Å
84 GPa

P6/mmm
a=2.43866(272) Å
c=2.26488(216) Å
105 GPa

Intensity (Arb. units)

2Θ (deg.)

Figure 1   LX12039   16Feb2011

(a) β-tin   (b) Imma   (c) sh
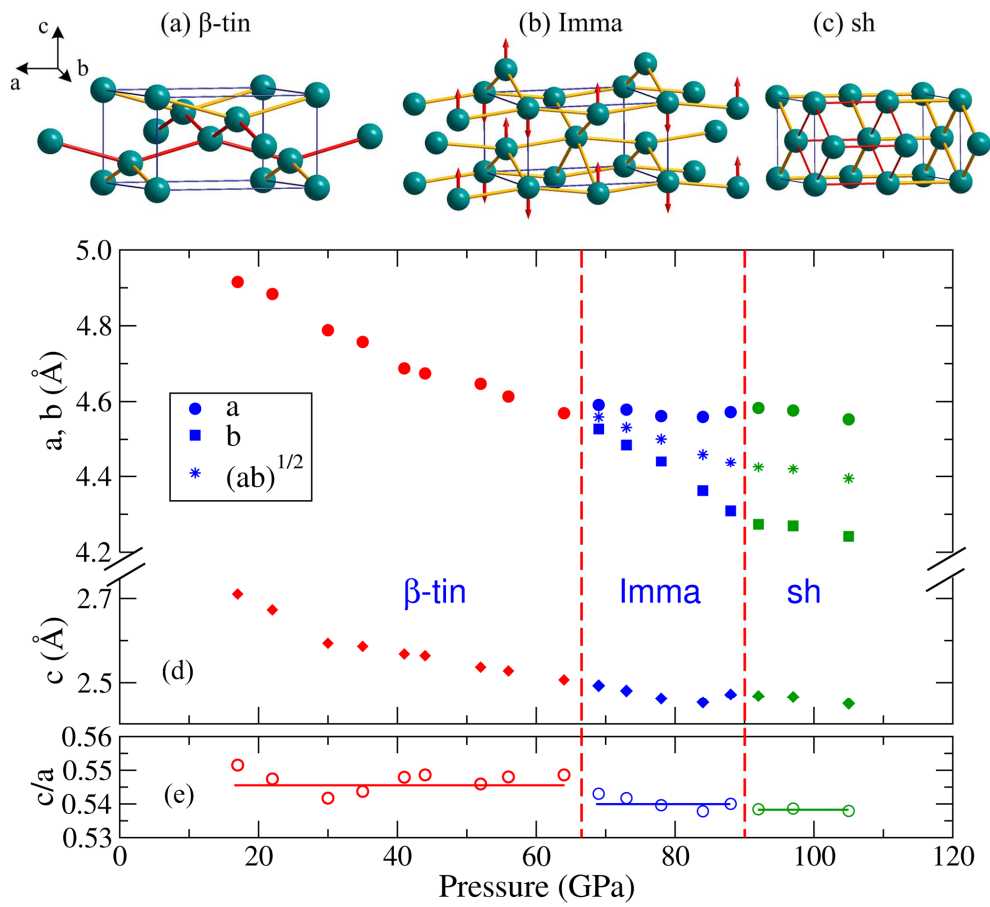
Figure 2   LX12039   16Feb2011
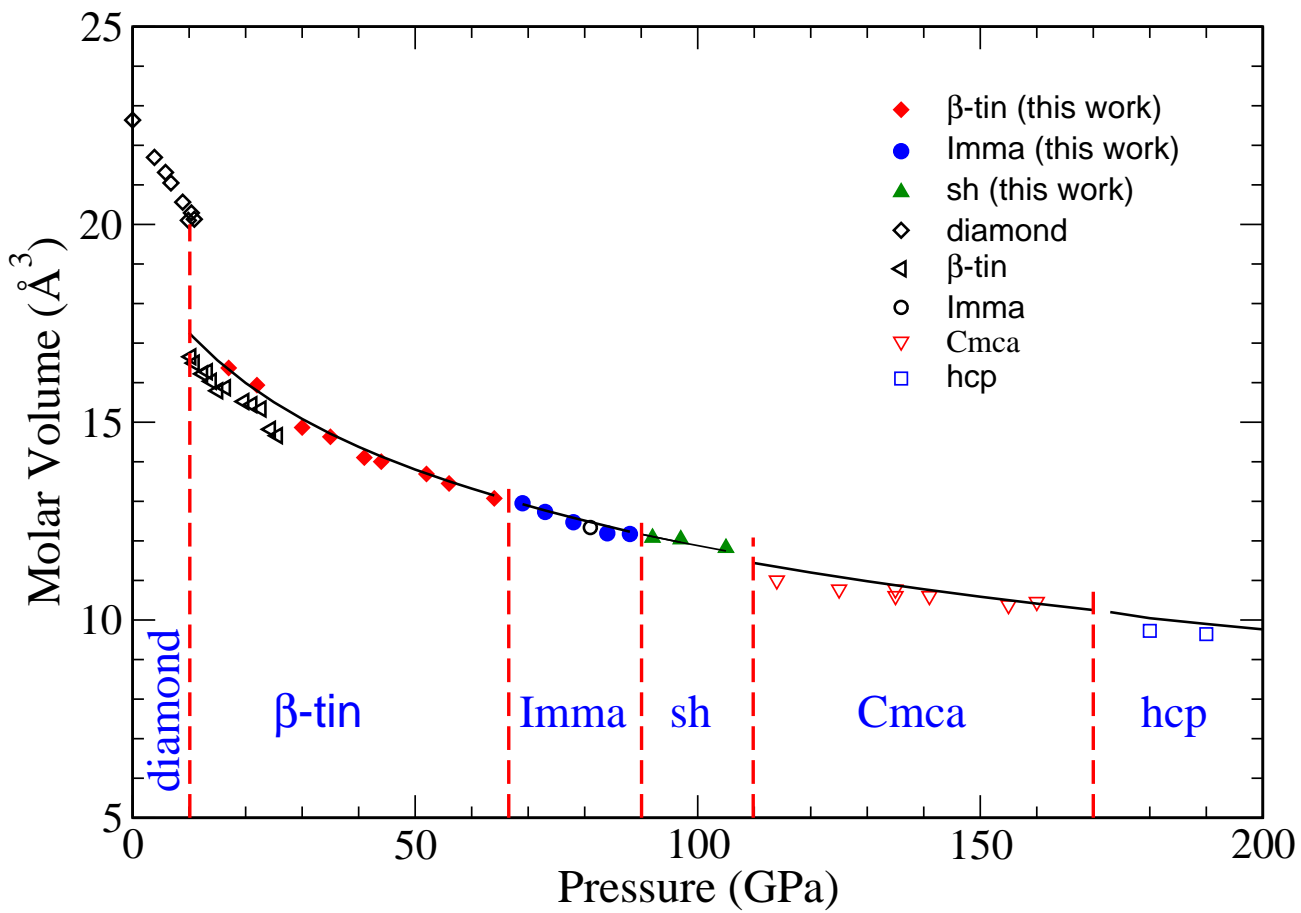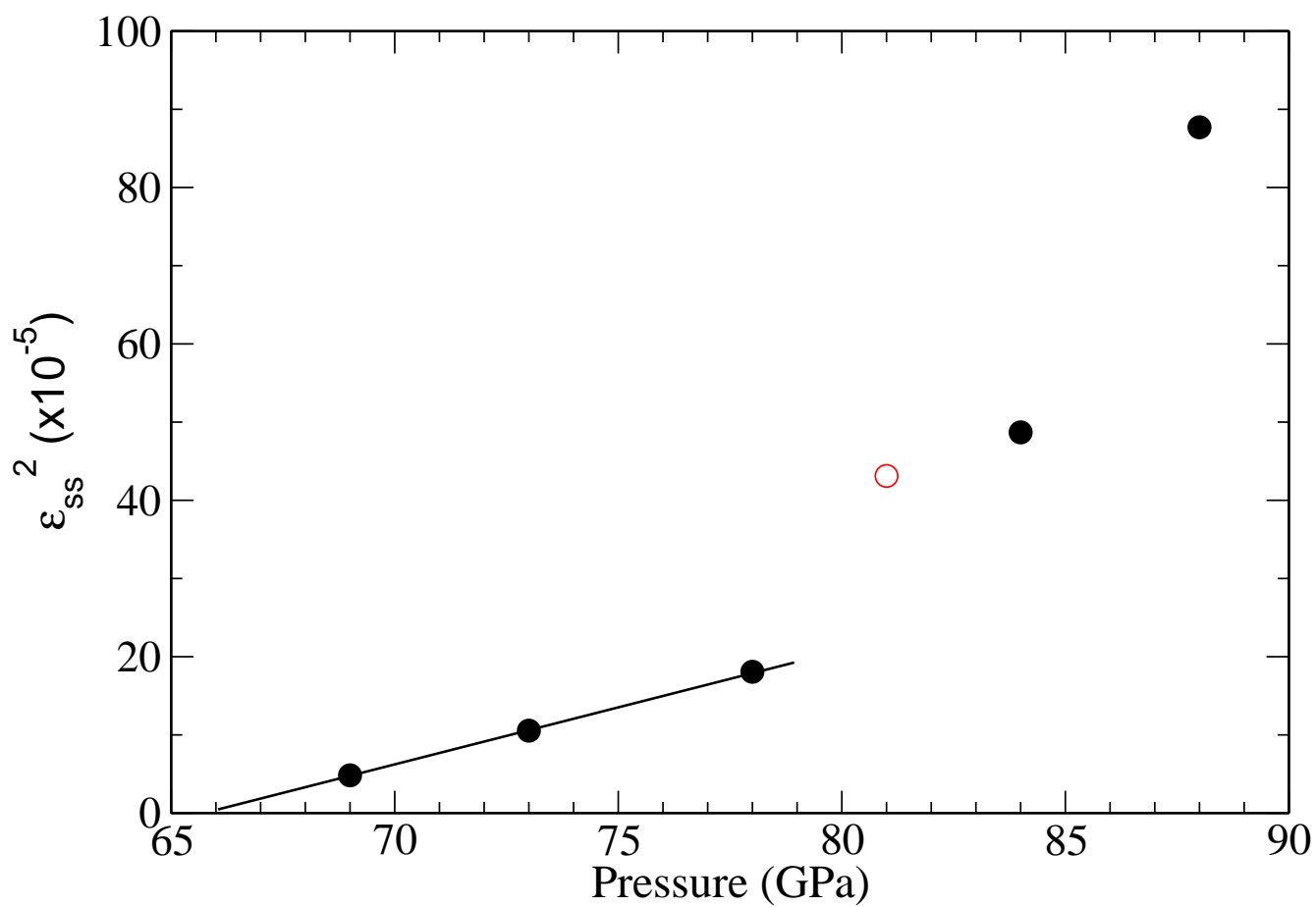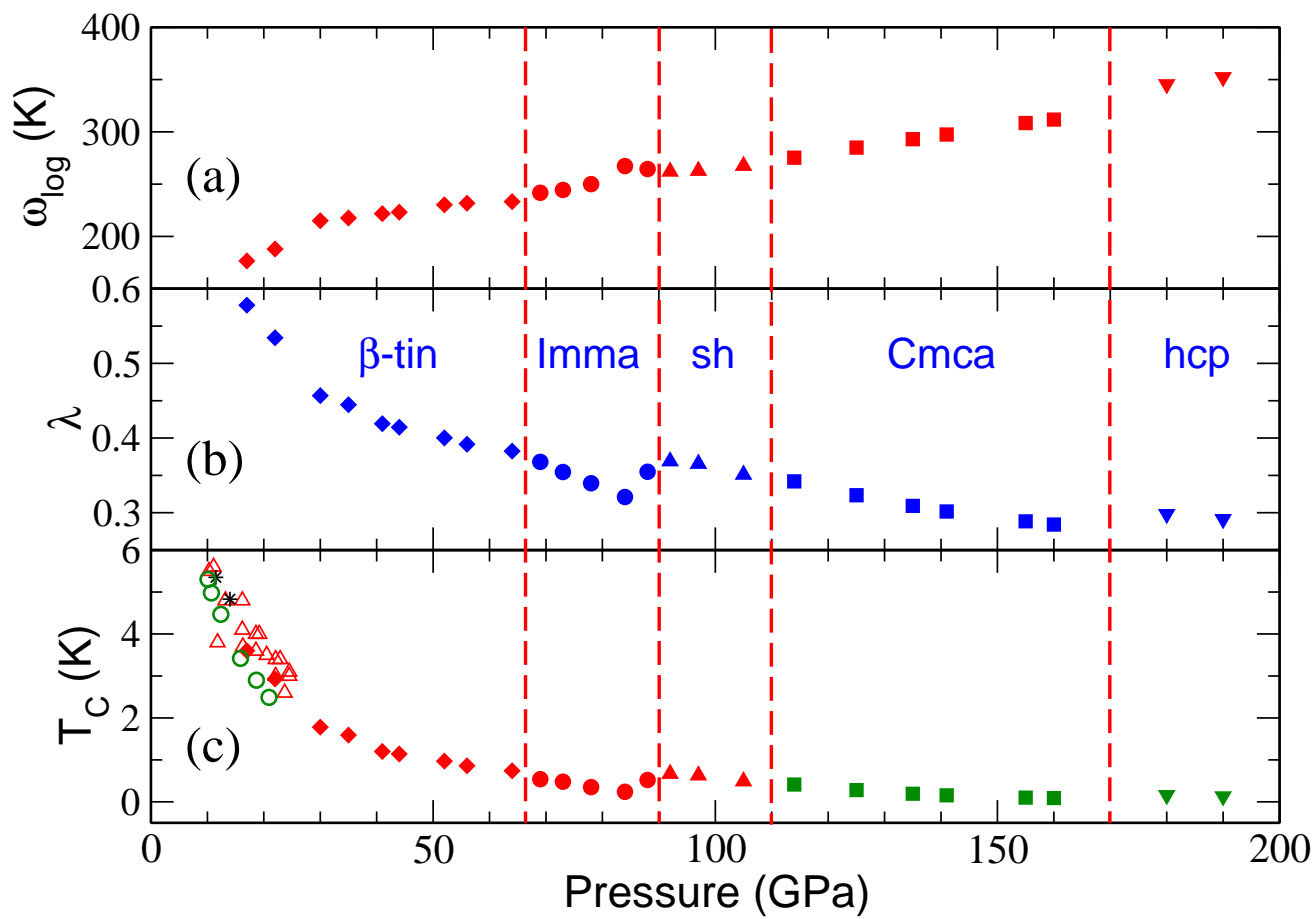
Figure 3   LX12039   16Feb2011

Figure 4   LX12039   16Feb2011

Figure 5   LX12039   16Feb2011